Phenotypic spectrum in osteogenesis imperfecta due to mutations in TMEM38B: unravelling a complex cellular defect

Webb, Emma; Balasubramanian, Meena; Fratzl-Zelman, Nadja; Cabral, Wayne A; Titherage, Hannah; Alsaedi, Atif; Saraff, Vrinda; Vogt, Julie; Cole, Trevor; Stewart, Susan; Crabtree, Nicola; Sargent, Brandi M; Gamsjaeger, Sonja; Paschalis, Eleftherios P.; Roschger, Paul; Klaushofer, Klaus; Shaw, Nick J.; Marini, Joan C; Högler, Wolfgang

DOI:
10.1210/jc.2016-3766

Document Version
Peer reviewed version

Citation for published version (Harvard):
Webb, E, Balasubramanian, M, Fratzl-Zelman, N, Cabral, WA, Titherage, H, Alsaedi, A, Saraff, V, Vogt, J, Cole, T, Stewart, S, Crabtree, N, Sargent, BM, Gamsjaeger, S, Paschalis, EP, Roschger, P, Klaushofer, K, Shaw, NJ, Marini, JC & Högler, W 2017, 'Phenotypic spectrum in osteogenesis imperfecta due to mutations in TMEM38B: unravelling a complex cellular defect', *The Journal of clinical endocrinology and metabolism*, vol. 102, no. 6, pp. 2019-2028. https://doi.org/10.1210/jc.2016-3766

Phenotypic spectrum in osteogenesis imperfecta due to mutations in TMEM38B: unravelling a complex cellular defect

Webb, Emma; Balasubramanian, Meena; Fratzl-Zelman, Nadja; Cabral, Wayne A; Titherage, Hannah; Alsaedi, Atif; Saraff, Vrinda; Vogt, Julie; Cole, Trevor; Stewart, Susan; Crabtree, Nicola; Sargent, Brandi M; Gamsjaeger, Sonja; Paschalis, Eleftherios P.; Roschger, Paul; Klaushofer, Klaus; Shaw, Nicholas; Marini, Joan C; Högler, Wolfgang

Phenotypic spectrum in osteogenesis imperfecta due to mutations in *TMEM38B*: unravelling a complex cellular defect

Emma A. Webb, PhD[1,2], Meena Balasubramanian, MD[3], Nadja Fratzl-Zelman, PhD[4], Wayne A. Cabral, PhD[5], Hannah Titheradge, MRCPCH[6], Atif Alsaedi[6], Vrinda Saraff, MRCPCH[1], Julie Vogt, MBBS[6], Trevor Cole, MBChB[6], Susan Stewart[6], Nicola J. Crabtree, PhD[1], Brandi M. Sargent, BS[5], Sonja Gamsjaeger, PhD[4], Eleftherios P. Paschalis, PhD[4], Paul Roschger, PhD[4], Klaus Klaushofer, MD[4], Nick J. Shaw, MBChB[1,2], Joan C. Marini, MD, PhD[5], Wolfgang Högler, DSc MD[1,2]

Affiliations

[1] Department of Endocrinology & Diabetes, Birmingham Children's Hospital, Birmingham, United Kingdom;
[2] Institute of Metabolism and Systems Research, University of Birmingham, and Centre for Endocrinology, Diabetes and Metabolism, Birmingham Health Partners, Birmingham, United Kingdom;
[3] Sheffield Clinical Genetics Service, Sheffield Children's NHS Foundation Trust, United Kingdom;
[4] Ludwig Boltzmann Institute of Osteology at Hanusch Hospital of WGKK, Vienna, Austria and AUVA Trauma Centre Meidling, 1st Med. Dept., Hanusch Hospital Vienna, Austria;
[5] Section on Heritable Disorders of Bone and Extracellular Matrix, NICHD, National Institutes of Health, Bethesda, USA
[6] Dept of Clinical Genetics, Birmingham Women's Hospital, Birmingham, United Kingdom;

Corresponding author (including contact information)

PD Dr. Wolfgang Högler

Department of Endocrinology & Diabetes, Birmingham Children's Hospital,

Steelhouse Lane, Birmingham, B4 6NH, United Kingdom

Tel: +44 (0)121 333 8197 Fax: +44 (0)121 333 8191

E-mail: wolfgang.hogler@bch.nhs.uk

Key words: osteogenesis imperfecta; osteoporosis; bone fragility; bone matrix mineralisation; TMEM38B; TRIC-B

Short title: Type XIV OI: Unravelling a complex cellular defect

Disclosures: EAW, MB, NFZ, WAC, AA, VS, JV, TC, SS, NC, BMS, SG, EPP, PR, KK, NJS, JM and WH have nothing to declare. Dr. Titheradge reports grants from UCB Pharma, during the conduct of the study.

Supplemental data: *Supplementary Figures 1 and 2, Supplementary Table 1, Supplementary Information 1*

Abstract

Context:

Recessive mutations in *TMEM38B* cause type XIV osteogenesis imperfecta (OI) by dysregulating intracellular calcium flux.

Objectives:

Clinical and bone material phenotype description and osteoblast differentiation studies.

Design and Setting:

Natural history study in paediatric research centres.

Patients:

Eight patients with type XIV OI.

Main Outcome Measures:

Clinical examinations included: bone mineral density, radiographs, echocardiography and muscle biopsy. Bone biopsy samples (n=3) were analysed using histomorphometry, quantitative backscattered electron microscopy and Raman microspectroscopy. Cellular differentiation studies were performed on proband and control osteoblasts and normal murine osteoclasts.

Results:

The clinical phenotype of type XIV OI ranges from asymptomatic to severe. Previously unreported features include vertebral fractures, periosteal cloaking, coxa vara and extraskeletal features (muscular hypotonia, cardiac abnormalities). Proband L1-L4 bone density Z-score was reduced (median -3.3 [range -4.77 to +0.1; n=7]), and increased by +1.7 (1.17 to 3.0; n=3) following bisphosphonate therapy. *TMEM38B* mutant bone has reduced trabecular bone volume, osteoblast and particularly osteoclast numbers, with

>80% reduction in bone resorption. Bone matrix mineralization is normal and nanoporosity low. We demonstrate a complex osteoblast differentiation defect with decreased expression of early markers and increased late and mineralization-related markers. Predominance of TRIC-B over TRIC-A expression in murine osteoclasts supports an intrinsic osteoclast defect underlying low bone turnover.

Conclusions:

OI type XIV has a bone histology, matrix mineralization and osteoblast differentiation pattern that is distinct from OI with collagen defects. Probands are responsive to bisphosphonates and some show muscular and cardiovascular features possibly related to intracellular calcium flux abnormalities.

INTRODUCTION

Osteogenesis Imperfecta (OI) is a clinically and genotypically heterogeneous, heritable connective tissue disorder which results in fragile, deformed bones, short stature and low bone mass (1). Most cases of OI are due to dominantly inherited mutations in *COL1A1* or *COL1A2* which affect the structure or quantity of type I collagen (Types I-IV) (2,3). Rare, mostly recessive, forms of OI are caused by defects in genes whose products are involved with collagen folding or post-translational modification (2,4-7).

Recessively inherited mutations in the *TMEM38B* gene (OMIM#611236), which encodes the ubiquitously expressed ER protein Trimeric Intracellular Cation channel type B (TRIC-B), cause OI type XIV (OMIM #615066). *TMEM38B* mutations reported to date include an exon 4 deletion among Bedouins (8,9), an exon 1-2 deletion in an Albanian child (10) and two point mutations in exon 4 and intron 3 in three Chinese children (11). Using primary fibroblasts and osteoblasts from affected individuals, we recently demonstrated that absence of TRIC-B disrupts ER calcium flux kinetics, consistent with increased activation of the PERK/ATF4 pathway of ER stress (12,13). Expression of multiple genes for collagen-interacting proteins is altered in proband cells, leading to dysregulated type I collagen synthesis, including decreased hydroxylation of collagen helical lysine residues and intracellular retention of misfolded collagen (12). The full clinical and skeletal phenotype, bone histomorphometry, bone material properties, osteoblast differentiation pattern and response to bisphosphonate (BP) therapy have not previously been presented.

MATERIAL AND METHODS

Clinical Data, Samples and Bone Imaging

Clinical information and anthropometric data were taken from medical records of six patients

(P1-6) with genetically confirmed type XIV OI attending OI specialist clinics at Birmingham Children's Hospital, Birmingham, UK; two brothers (P7,8) were studied at the NIH Clinical Center, Bethesda, MD, USA. In both centers, all patients with clinical signs suggestive of OI are offered genetic testing using a recessive OI gene panel. Blood, bone biopsy and DNA samples were collected from the patients and their parents after obtaining informed consent/assent. Bone densitometry, including lateral vertebral assessment (Hologic or GE Lunar iDXA™), and X-rays were taken as part of routine clinical care or OI natural history protocols. Lateral vertebral morphometry was assessed using the Genant score (14).

Bone tissue characteristics: Bone Histomorphometry, quantitative Backscattered Electron Imaging (qBEI) and Raman Microspectroscopy

Trans-iliac bone biopsies were taken in patients 2, 4 and 7 (when naïve to BP therapy) and repeated in P7 after one year of BP therapy. Double-labeling with tetracycline for dynamic measurement of bone formation was performed in P2 and P7. Sample preparation and histomorphometric analyses were performed using standard procedures (15). Bone mineralisation density distribution (BMDD), reflecting the calcium content of bone matrix, was measured in trabecular and cortical bone by qBEI as described previously (16).

Raman microspectroscopy was used to evaluate the properties of the trabecular bone mineral and organic matrix as a function of 4 tissue ages (17,18): i) between the 2nd fluorescent label and the mineralizing front (1-3 day-old bone), ii) between the two fluorescent labels (4-20 day-old bone), iii) immediately behind the 1st fluorescent label (over 20 day-old bone), and, iv) the geometrical centre of trabeculae (older bone tissue). At each tissue age, the mineral/matrix ratio, nanoporosity (a surrogate of tissue water), glycosaminoglycan, lipid and pyridinoline content were determined, as previously described (18). Results from bone

histomorphometry, qBEI and Raman analysis were compared to paediatric reference data from healthy subjects, and type I OI patients (17,19-23).

Molecular Studies

Genomic DNA was extracted using standard protocols. For P1-6, clonal sequencing using SureSelect target enrichment (Agilent Technologies) and the Illumina MiSeq platform was performed using a custom designed gene panel. Sequence analysis using a custom bioinformatics pipeline based on open source workflow by the Broad Institute (http://www.broadinstitute.org/gatk/guide/best-practices) was undertaken using a minimum threshold of 30-fold read depth for exonic sequence and intron/exon boundary. Variants identified were filtered against polymorphism lists and assessed using the Association for Clinical Genetic Science Best Practice Guidelines (http://www.acgs.uk.com). For P7 and P8, the maternal *TMEM38B* mutation was detected by NGS using a recessive OI panel (CTGT, Allentown, PA, USA). Subsequently, the paternal mutation was detected by deletion analysis (12).

Cell Culture

Primary osteoblast (OB) cultures were established from surgical bone chips of normal control (aged 4 years) and P7 (prepubertal, aged 13 years), as previously described (24). To induce OB differentiation, confluent cells were cultured for 30 days in αMEM, supplemented with 10% fetal bovine serum, 1% pen-strep, 25 μg/mL L-ascorbic acid, 10^{-8} M dexamethasone and 2.5 mM 2-glycerophosphate.

Bone marrow-derived primary osteoclast (OC) cultures were generated from femora of 8-week BL/6 mice as previously described (25). Cultures were assessed for an OC phenotype by the presence of multinucleated TRACP-positive stained cells (Sigma).

Analysis of Gene Expression

Total RNA was extracted from patient OB and mouse OC cultures at the indicated time points using TriReagent (Molecular Research Center) according to the manufacturer's protocol, then treated with DNA-free (Life Technologies). Gene transcript levels of cell differentiation markers were quantitated by real-time RT-PCR following reverse-transcription using a High Capacity cDNA Archive Kit and Taqman Assays on Demand (**Suppl. Information 1**). Relative expression of genes of interest was measured in triplicate and normalized to 2 reference genes (*ACTB*, *B2M*, *Actb*, and *B2m*).

RESULTS

Molecular Studies

P1-6 originated from three apparently unrelated Pakistani families living in Birmingham, UK, and presented with increased bone fragility and osteoporosis. Sanger sequencing confirmed that all probands were homozygous for the same c.507G>A mutation in exon 4 of *TMEM38B*. This mutation replaces tryptophan169 with a STOP codon (p.W169X). All obligate carrier parents were heterozygous for the mutation (**Suppl. Figure 1**).

P7 and P8 were born to unrelated American parents of British/Scottish and British/German origin and found to be compound heterozygous for the previously reported deletion encompassing *TMEM38B* exons 1 and 2 (10) and a novel c.63dupT, which directly introduces a premature termination codon (p.D22X). Their father carries the deletion and their mother the c.63dupT allele.

Both genotypes lead to a *TMEM38B* null molecular outcome in fibroblast and OB cultures of patients P2 and P7 (who appear as Probands 3 and 2 respectively, in (12)).

Clinical and Radiological Phenotype

Expressivity of clinical OI features was highly variable (**Table 1**). P1 and P6 presented antenatally with bowed femora. P1-7 had sustained a significant low trauma fracture by 2 years of age, whilst P8 had no fractures. Two individuals were short (height < -2 SDs) and overweight. P5 had non-progressive bilateral nephrocalcinosis of unknown origin detected at birth. P7 has relative macrocephaly (58cm, 98th centile) with normal brain MRI, facial appearance and dentition. His clinical OI phenotype was severe whilst his brother (P8) was asymptomatic, indicating incomplete penetrance. All had normal calcium and phosphate metabolism, only P2 had consistently elevated alkaline phosphatase (ALP) levels.

Cognitive Development

P1 and P2 developed motor skills appropriately but have delayed speech and language development. P2 has a concomitant diagnosis of autistic spectrum disorder. Cognitive development is normal in P3-8.

Radiological Findings

Long bone radiographs of all patients demonstrated osteopenia (**Suppl. Figure 2**). Five patients required femoral rodding (**Table 1**). Interestingly, P1 whose radiographs at birth showed femoral bowing with mid-shaft cortical thickening, developed widespread periosteal reactions ('cloaking') of all long bones at 2 months of age. A follow-up skeletal survey at 22 months of age showed resolving periosteal reaction, coxa vara and osteopenia (**Suppl. Figure 2 A-C, E, F, H, I**). In contrast, P7 has extremely thin long bones (**Suppl. Figure 2 N, O**). P1 had 4-5 Wormian bones around the lambdoid suture at age 2 months.

Spine and Respiratory

P1 had multiple vertebral compression fractures at age 2 months which showed incomplete reshaping by 22 months (**Suppl. Figure 2 A, D, G**). P2 had multiple vertebral compression fractures at presentation aged 12 years (**Suppl. Figure 2 J**). To date, two patients (25%) have developed scoliosis (Cobb angle >10˚), which is progressively deforming in P5 and P7. Following spinal rodding surgery at age 15 years, P5 has severe restrictive lung disease. P7 developed moderate lower airway obstruction with air trapping at age 22 years (**Table 1**).

Cardiovascular Health

Three patients (P3,5,7) displayed cardiac pathology. P3 presented aged 14 years with secondary amenorrhea, significant weight gain (BMI 32kg/m^2) and hirsutism. She had impaired glucose tolerance (120 min glucose 10.4mmol/L post oral glucose load), acanthosis nigricans, and fatty liver on ultrasound. She was started on metformin and later on a combined ethinylestradiol/cyproterone acetate contraceptive pill (COCP), on which her hirsutism, weight gain and periods improved. Aged 16 years, she had an extensive anterior myocardial infarction secondary to a thrombus in the left anterior descending coronary artery. Her COCP was discontinued. P5 had a large congenital secundum atrial septal defect and a perimembraneous ventricular septal defect. He developed heart failure, requiring surgery aged 2 months. P7's echocardiogram aged 21 years revealed tricuspid regurgitation with an anatomically normal valve. At age 27, asymmetric septal hypertrophy of the left ventricle and mild aortic root dilation were detected. The septal hypertrophy progressed further and he developed non-obstructive hypertrophic cardiomyopathy with ST elevation and borderline right axis deviation on ECG. Cardiovascular lipid profile was normal in all eight individuals. Echocardiogram and ECG were normal in P1,2,4-6,8.

Muscle Phenotype

P1-3 and P6, their unaffected siblings, and P7 and P8 have no evidence of myopathy. P4 has muscular hypotonia, which was fully investigated. Her EMG showed a denervating pattern with no suggestion of muscle myopathic activity. Muscle biopsy also showed no evidence of congenital myopathy, metabolic or storage disorder or mitochondrial cytopathy. Serum lactate, basic mitochondrial DNA screen and MRI brain were normal. She walks with a Trendelenburg gait. Her brother, P5, also has moderate hypotonia associated with delayed motor milestones, and only walked without support at 3 years of age.

Clinical and radiological phenotype of heterozygous carriers

Parents of affected patients had no history of fractures, were generally healthy, with normal lumbar spine bone density (BMD) where measured (Z-scores: 0.7 to -0.3, n=4). Parents of P7/8 were fully assessed. Their father, age 59 years, has macrocephaly (59cm, >95th centile), moderate hip laxity, degenerative changes in mid-thoracic vertebrae, normal BMD (Z-score +0.1), and occupational high-frequency hearing loss bilaterally. Echocardiogram shows concentric left ventricular hypertrophy, mildly dilated ascending aorta, and mild mitral and aortic regurgitation with normal valvular anatomy. Their mother, age 56 years, has type I DM and Graves' Disease, short stature and normal head circumference. Radiographs show mild central compressions of lower thoracic and lumbar vertebrae, with normal BMD (Z-score -0.3). Calcifications were noted in the abdominal aorta on X-rays, with annular calcification of mitral and aortic valves. She has mild mid-frequency sensorineural hearing loss bilaterally.

Bone mineral density and response to BP treatment

Proband lumbar spine BMD Z-scores varied widely, ranging from normal (P3,4) to osteopenic (P6,8) to decreased (P2,5,7) with mean median Z-score -3.3 [range -4.77 to +0.1]) in individuals old enough to be measured (P2-8, **Table 2**). Four patients were

treated with BPs. DXA scans before and after treatment (n=3) revealed substantial increase in BMD Z-score of 3, 1.7 and 1.17 SD (median +1.7), respectively. Patients with BMD Z-scores within the normal range have not required BP treatment to date.

Evaluation of trans-iliac bone biopsies

A) Bone histomorphometry (Table 3)

The main histomorphometric features in the trans-iliac biopsy samples (P2,4,7) were predominance of low BV/TV, normal to reduced OB numbers and very low resorption. Backscattered electron images demonstrate bone volumes (BV/TV) below -1SD in P4 **(Figure 1C)** and below -4SD (-82% from normal) in P7 (**Figure 1D)**. Whilst BV/TV could not be assessed in P2, many thin and partially isolated trabecular features were viewed in the cancellous compartment (**Figure 1A, B)**. Trabecular surfaces (in P2 and P7) were covered by an abnormally extended and thin osteoid layer resulting in a substantial increase in osteoid surface (OS/BS) and osteoid volume (OV/BV) (**Table 3**). Unlike OI caused by collagen-gene mutations, neither OB nor OC indices were increased in affected patients. In fact, OB surface (Ob.S/BS) and mineralizing surface (MS/BS) were within normal range or decreased (P4). Interestingly, despite the low amount of trabecular bone, intense fluorescent double labels were detected in cortical bone (**Figure 1E**, P7). P2 had focal areas of osteoid accumulation which explains the elevated mineralization lag time (Mlt) and the low adjusted apposition rate (aj.AR). In all patients, OC and bone resorption indices were markedly decreased to less than 20% of healthy controls. Bone cortex had a normal thickness, lamellar pattern, and normal haversian canals.

B) qBEI (Table 4)

Trabecular bone:

In P2 and P7, the average bone matrix mineralization was normal, rather than elevated as in

OI type I bone. The matrix portion with low mineralization (CaLow) was slightly above both the healthy reference and OI type I ranges. In contrast, P4 had a BMDD curve that was shifted towards higher matrix mineralization (**Figure 1F**) with increased CaMean, CaPeak and CaHigh values, consistent with low turnover revealed on histomorphometry. In all patients, the portion of fully mineralized CaHigh was markedly lower (53-84%) than in OI type I.

Cortical bone:

The CaMean and CaPeak of P2 and P4 were within the normal range, although again P4 showed increased CaHigh. In contrast, P7's cortical bone matrix before BP treatment was much less mineralized than control bone, even less than his trabecular bone (CaMean: -7%, and -10% respectively). Concomitantly, there was a 3-fold increase of CaLow reflecting the large portion of bone undergoing primary mineralization. The high cortical bone apposition was mirrored by strong tetracycline labeling on endo –and intracortical surfaces (**Figure 1E**). After one year of BP therapy, P7's cortical CaMean and CaPeak increased and CaLow decreased substantially, reflecting increasing tissue age due to the anticatabolic therapy.

C) Raman Microspectroscopy

Mineral/matrix and mineral maturity/crystallinity ratios were within reference range of healthy children. Nanoporosity was decreased (at younger tissue ages in P2, P7 and oldest in P4), compared to healthy controls and even lower than classical OI bone. Relative glycosaminoglycan content at the oldest tissue age was decreased in P2,4 and increased in P7 compared to healthy children. Lipid content was lower in P2 and P7 compared to healthy children. Finally, pyridinoline content was comparable to OI type I bone, being higher than normal at the two younger tissue ages, and normal at older ones (**Suppl. Table 1**).

Osteoblast and osteoclast studies

Cultured osteoblasts from P7 showed reduced expression of early markers of differentiation (*RUNX2*, *SP7*, *COL1A1*, *SPARC*), an increase in later markers, including those related to mineralization (*ALPL*, *OPN*, *IBSP*, *BGLAP*, *DMP*) and also delayed *SOST* expression (**Figure 2**). The normal *RANKL*/*OPG* profile suggests normal functioning of the major extrinsic OC stimulation system. To explain the low bone resorption on patient bone histomorphometry, we examined osteoclasts from murine cultures, since cultures of patient osteoclasts were not available. We determined whether *Tric-b* and its coupled [Ca^{2+}] channel Itpr3 were expressed in differentiated murine osteoclasts, as well as the potential for redundancy by *Tric-a* and its coupled Ryr3 [Ca^{2+}] channel in this cell type (26). The results confirm marked predominant expression of the ER TRIC-B channel over TRIC-A (10-15-fold in mature OC), and the IP_3R3 [Ca^{2+}] efflux channel over RyR3 (≈ 25-fold), respectively (**Figure 2, bottom panels**).

DISCUSSION

TMEM38B null mutations cause type XIV OI by disturbing ER calcium flux kinetics, which alters the function of multiple proteins in the ER (12). Type I collagen post-translational modification displays a distinct pattern, with decreased helical and increased telopeptide lysyl hydroxylation, which contrasts with the helical over-modification typical of classical dominant OI and recessive defects in procollagen prolyl 3-hydroxylation. Procollagen in *TMEM38B*-null cells is also misfolded and substantially degraded intracellularly, underlying reduced collagen secretion (12). Here, we present our extensive investigations of the type XIV OI phenotype, its distinctive bone tissue characteristics and bone cellular defects.

The skeletal phenotype of our eight patients had variable expressivity and penetrance, ranging from barely detectable to severe. Development of scoliosis and hearing loss was also variable. We observed previously unreported features such as vertebral fractures with spontaneous reshaping, periosteal cloaking, coxa vara and abnormal dentition. Periosteal cloaking similar to our observation in P1 appears present on radiographs of other patients with OI type XIV (8) and OI of unknown etiology (27). Such generalised cloaking may represent a response to healing long bone fractures and is not typical of classical OI. Cardiac abnormalities of different etiologies were observed in three patients, and in both carrier parents of P7/8. P4 and P5 have muscular hypotonia. However, muscle and myocardial cells express much more TRIC-A than the ubiquitous TRIC-B (28), although TRIC-B deficiency may indirectly affect these tissues via increased ER stress. *Tric-a* and *Tric-b* double KO mice die *in-utero* due to cardiac arrest, indicating a shared role of these channels in Ca^{2+} signalling in embryonic cardiomyocytes. In addition, even *Tric-b*$^{+/-}$ mice are susceptible to stress-induced heart failure (28), which potentially indicates an association between the cardiac findings and the heterozygous state of P7/8's parents. Until more evidence becomes available, monitoring cardiovascular risk factors in affected patients may be required. In addition, the lack of significant respiratory abnormalities in our patients contrasts with the *Tric-b* KO mouse model, which shows respiratory defects with abnormal IP_3R-mediated Ca^{2+} release in airway epithelial cells. Finally, in view of parental consanguinity, we cannot confidently attribute cognitive impairment in P1 and P2 to a *TMEM38B* effect in neuroepithelial tissue.

OI type XIV bone is structurally distinct from bone with type I collagen gene defects. In the absence of TRIC-B, bone tissue has low-normal OB numbers with a low mineral apposition rate (Aj.AR) and a uniform paucity of OCs. In classical OI, bone turnover and cell numbers

are high, but mineral apposition rate is low, implying that many OBs produce less matrix, which is typically hypermineralized (23,29). BMDD by qBEI in TRIC-B deficient bone is either normal or slightly right-shifted, reflecting a situation of low bone turnover that allows more time for bone packets to mineralize (16,30). Specifically P4 has a high mineralization, low turnover profile similar to children with chronic kidney disease or slow growth (31). In contrast, bone from P7, with the most severe skeletal phenotype, featured active OBs on rudimental trabeculae, a lack of OCs but normal BMDD. Strikingly, his cortex showed active primary bone formation as evidenced by intense intra- and endocortical fluorescence labeling (**Figure 2E**) and increased cortical CaLow. Raman microspectroscopy also revealed an unaltered mineral/matrix ratio in *TMEM38B* mutant bone. However, similar to classical OI bone, nanoporosity, a surrogate of tissue water, was decreased at the three younger tissue ages compared to healthy controls (22). Consistently, elevated pyridinoline content at the two younger tissue ages mirrors increased or accelerated trivalent cross-links formation resulting in stiffer collagen fibers, which exhibit more "brittle-like" behavior (32). Thus, bone fragility in type XIV OI is explained by reduced trabecular bone and nanoporosity, and increased pyridinoline content. Despite low bone resorption, bone mineral density and cortical mineral content increased in response to BP therapy in Type XIV OI patients. The observed shift towards higher, and less heterogeneous, cortical BMDD following one year of BP therapy is characteristic for patients with normal or lowered mineralization density (16). This contrasts sharply to classical OI bone where the hypermineralized, fully saturated matrix cannot further increase its density (29).

Differentiation of P7's osteoblasts demonstrated reduced expression of early markers of differentiation (*RUNX2*, *SP7*, and *COL1A1*), which is consistent with reduced OB numbers shown on bone biopsy, and would exacerbate the decreased collagen secretion resulting from

collagen misfolding in the ER (12). Expression of the OB differentiation marker ALP is related to [Ca^{2+}] flux since its suppression by siRNA blocks BMP2-induced flux of [Ca^{2+}] from ER to cytoplasm, raising the proposal of ALP as a monitor of intracellular calcium concentration (33). Our cell culture work suggests that this loop may also work in the reverse direction, with reduced ER [Ca^{2+}] flux in TRIC-B deficient cells leading to a compensatory increase in osteoblast *ALPL* expression.

Calcium signalling has broad effects on pathways promoting and inhibiting mineralization. Expression of multiple genes whose products interact with [Ca^{2+}] and/or influence mineralization are altered in Type XIV OI osteoblasts, although mineralization of type XIV OI bone tissue is not abnormal. Whilst expression of pro-mineralization ALP/*ALPL* (34) is increased, there is decreased expression of osteonectin/*SPARC*, which initiates and promotes mineralization, and increased expression of osteocalcin/*BGLAP* and *OPN*, which inhibit crystal growth (35,36). The SIBLING proteins BSP and OPN have generally opposing roles in promoting and opposing mineralization (37), but their concurrent increase in transcripts in TRIC-B deficient cells is unexpected, since *BSP*$^{-/-}$ cells have increased OPN expression (38). Further, *SOST* expression was delayed, suggesting differentiation to osteocytes may be impaired. The complex OB gene expression pattern apparently contravenes the usual OI mechanism toward hypermineralization. Studies on the levels and interactions of these proteins in TRIC-B deficient cells and matrix should be a focus of further investigation. In partial agreement with our patient findings, differentiated calvarial OBs of *Tric-b* KO mice have normal levels of type I collagen transcripts, with decreased collagen production due to intracellular degradation (26). As in patient cells, the early differentiation markers *Runx2* and *Osx* are reduced in murine OBs. However, *Alpl*, *Bsp* and *Bglap* transcripts are reduced, while *Sparc* is normal, suggesting greater impairment of murine OB differentiation and mineralization than in patients.

An apparent intrinsic defect in osteoclasts is another distinctive feature of Type XIV OI. To investigate the low OC numbers and activity in patient bone in the context of normal osteoblast *RANKL*/*OPG* ratios, we investigated the levels of expression of the *TRIC-B/IP3R* and *TRIC-A/RyR* paired sets of channels for K^+ entry and Ca^{2+} efflux from the ER in normal murine OCs. Our demonstration of 15-fold higher expression of TRIC-B relative to TRIC-A, and 25-fold higher expression of IP_3R than RyR channels support the predominance of the TRIC-B system in osteoclasts, with minimal to no redundancy of function. Combined with patient histomorphometry and *in vitro* OB expression profiles, our data support an intrinsic, OB-independent, OC defect in patients with *TMEM38B* mutations. We speculate that interference with [Ca^{2+}] flux kinetics in TRIC-B null OCs impairs their response to normal developmental signals, resulting in low OC numbers, and reduced bone resorption. In recent experimental data from *Tric-b*$^{-/-}$ mice (26), OC markers such as cathepsin K and Atp6v0d2 had reduced expression in newborn murine femora.

In conclusion, we describe a wide phenotypic spectrum of OI caused by *TMEM38B* mutations, ranging from asymptomatic to severe and novel skeletal and potential extraskeletal features. Such phenotypic variability even with identical genotypes may reflect different ethnic and genetic backgrounds, modifiers of *TMEM38B* expression or other genes involved in post-translational modification and ER calcium flux. Whilst the small number of biopsies with great variability limits interpretation, bone turnover and BMDD were remarkably lower than in classical OI (23). Although normal BMDD has also been reported in OI caused by *WNT1* mutations (39), *WNT1*-deficient patients lack the abnormalities of type I collagen post-translational modification found in OI type XIV. The paucity of OBs and OCs, the normal BMDD with extremely reduced nanoporosity are uniquely different from

classical OI. Here, we further delineate the mechanism of bone fragility in *TMEM38B* mutant bone not only as a complex OB differentiation defect due to impaired ER Ca^{2+} flux kinetics, but also likely as an intrinsic OC defect. Despite the low bone resorption, patients still respond to BP therapy with increased BMD and cortical bone matrix mineralization. The role of TRIC-B in human OB and OC function, as well as cardiovascular or muscular health requires further study.

Acknowledgements

Authors' roles: Molecular studies: MB, AA, HT, WAC; Bone tissue studies: NFZ, SG, PR, EP, KK; Patient evaluation and reports: EW, WH, NS, VS, NC, TC, BMS, JCM; Drafting manuscript: EW, MB, NFZ, JCM, WH; Revising manuscript content: EW, MB, SS, HT, TC, WAC, PR, NFZ, KK, NC, NS, JCM, WH. We are grateful to Prof Eamonn Maher, University of Cambridge; Duncan McHale and Martin Armstrong, UCB Pharma; Professor David Goldstein and Slave Petrovski, Columbia University, for supervising Dr Titheradge's MD and enabling whole exome sequencing. We thank Dr Neil Gittoes, Queen Elizabeth Hospital Birmingham, for assisting with data collection. The authors thank Daniela Gabriel, Petra Keplinger, Sonja Lueger and Phaedra Messmer for careful sample preparations and qBEI measurements. This study was supported by the AUVA (Research funds of the Austrian workers compensation board) and by the WGKK (Viennese regional health insurance fund), and NICHD/NIH intramural funds to JCM.

References

1. Sillence DO, Rimoin DL. Classification of osteogenesis imperfect. Lancet 1978; 1:1041-1042

2. Van Dijk FS, Sillence DO. Osteogenesis imperfecta: clinical diagnosis, nomenclature and severity assessment. Am J Med Genet A 2014; 164A:1470-1481
3. Forlino A, Marini JC. Osteogenesis imperfecta. Lancet 2016; 387:1657-1671
4. Rohrbach M, Giunta C. Recessive osteogenesis imperfecta: clinical, radiological, and molecular findings. Am J Med Genet C Semin Med Genet 2012; 160C:175-189
5. Warman ML, Cormier-Daire V, Hall C, Krakow D, Lachman R, LeMerrer M, Mortier G, Mundlos S, Nishimura G, Rimoin DL, Robertson S, Savarirayan R, Sillence D, Spranger J, Unger S, Zabel B, Superti-Furga A. Nosology and classification of genetic skeletal disorders: 2010 revision. Am J Med Genet A 2011; 155A:943-968
6. Marini JC, Blissett AR. New genes in bone development: what's new in osteogenesis imperfecta. J Clin Endocrinol Metab 2013; 98:3095-3103
7. Marini JC, Reich A, Smith SM. Osteogenesis imperfecta due to mutations in non-collagenous genes: lessons in the biology of bone formation. Curr Opin Pediatr 2014; 26:500-507
8. Shaheen R, Alazami AM, Alshammari MJ, Faqeih E, Alhashmi N, Mousa N, Alsinani A, Ansari S, Alzahrani F, Al-Owain M, Alzayed ZS, Alkuraya FS. Study of autosomal recessive osteogenesis imperfecta in Arabia reveals a novel locus defined by TMEM38B mutation. J Med Genet 2012; 49:630-635
9. Volodarsky M, Markus B, Cohen I, Staretz-Chacham O, Flusser H, Landau D, Shelef I, Langer Y, Birk OS. A deletion mutation in TMEM38B associated with autosomal recessive osteogenesis imperfecta. Hum Mutat 2013; 34:582-586
10. Rubinato E, Morgan A, D'Eustacchio A, Pecile V, Gortani G, Gasparini P, Faletra F. A novel deletion mutation involving TMEM38B in a patient with autosomal recessive osteogenesis imperfecta. Gene 2014; 545:290-292
11. Lv F, Xu XJ, Wang JY, Liu Y, Asan, Wang JW, Song LJ, Song YW, Jiang Y, Wang O, Xia WB, Xing XP, Li M. Two novel mutations in TMEM38B result in rare autosomal recessive osteogenesis imperfecta. J Hum Genet 2016; 61:539-545
12. Cabral WA, Ishikawa M, Garten M, Makareeva EN, Sargent BM, Weis M, Barnes AM, Webb EA, Shaw NJ, Ala-Kokko L, Lacbawan FL, Hogler W, Leikin S, Blank PS, Zimmerberg J, Eyre DR, Yamada Y, Marini JC. Absence of the ER Cation Channel TMEM38B/TRIC-B Disrupts Intracellular Calcium Homeostasis and Dysregulates Collagen Synthesis in Recessive Osteogenesis Imperfecta. PLoS Genet 2016; 12:e1006156
13. Horiuchi K, Tohmonda T, Morioka H. The unfolded protein response in skeletal development and homeostasis. Cell Mol Life Sci 2016; 73:2851-2869
14. Genant HK, Wu CY, van Kuijk C, Nevitt MC. Vertebral fracture assessment using a semiquantitative technique. Journal of Bone and Mineral Research 1993; 8:1137-1148
15. Glorieux FH, Travers R, Taylor A, Bowen JR, Rauch F, Norman M, Parfitt AM. Normative data for iliac bone histomorphometry in growing children. Bone 2000; 26:103-109
16. Roschger P, Paschalis EP, Fratzl P, Klaushofer K. Bone mineralization density distribution in health and disease. Bone 2008; 42:456-466
17. Gamsjaeger S, Hofstetter B, Fratzl-Zelman N, Roschger P, Roschger A, Fratzl P, Brozek W, Masic A, Misof BM, Glorieux FH, Klaushofer K, Rauch F, Paschalis EP. Pediatric reference Raman data for material characteristics of iliac trabecular bone. Bone 2014; 69:89-97

18. Paschalis EP, Fratzl P, Gamsjaeger S, Hassler N, Brozek W, Eriksen EF, Rauch F, Glorieux FH, Shane E, Dempster D. Aging Versus Postmenopausal Osteoporosis: Bone Composition and Maturation Kinetics at Actively-Forming Trabecular Surfaces of Female Subjects Aged 1 to 84 Years. Journal of Bone and Mineral Research 2016;31(2):347-57
19. Rauch F, Travers R, Parfitt AM, Glorieux FH. Static and dynamic bone histomorphometry in children with osteogenesis imperfecta. Bone 2000; 26:581-589
20. Fratzl-Zelman N, Roschger P, Misof BM, Pfeffer S, Glorieux FH, Klaushofer K, Rauch F. Normative data on mineralization density distribution in iliac bone biopsies of children, adolescents and young adults. Bone 2009; 44:1043-1048
21. Glorieux FH, Rauch F, Plotkin H, Ward L, Travers R, Roughley P, Lalic L, Glorieux DF, Fassier F, Bishop NJ. Type V osteogenesis imperfecta: a new form of brittle bone disease. Journal of Bone and Mineral Research 2000; 15:1650-1658
22. Paschalis EP, Gamsjaeger S, Fratzl-Zelman N, Roschger P, Masic A, Brozek W, Hassler N, Glorieux FH, Rauch F, Klaushofer K, Fratzl P. Evidence for a Role for Nanoporosity and Pyridinoline Content in Human Mild Osteogenesis Imperfecta. Journal of Bone and Mineral Research 2016; 31:1050-1059
23. Roschger P, Fratzl-Zelman N, Misof BM, Glorieux FH, Klaushofer K, Rauch F. Evidence that abnormal high bone mineralization in growing children with osteogenesis imperfecta is not associated with specific collagen mutations. Calcif Tissue Int 2008; 82:263-270
24. Robey PG, Termine JD. Human bone cells in vitro. Calcif Tissue Int 1985; 37:453-460
25. Kang H, Chang W, Hurley M, Vignery A, Wu D. Important roles of PI3Kgamma in osteoclastogenesis and bone homeostasis. Proc Natl Acad Sci U S A 2010; 107:12901-12906
26. Zhao C, Ichimura A, Qian N, Iida T, Yamazaki D, Noma N, Asagiri M, Yamamoto K, Komazaki S, Sato C, Aoyama F, Sawaguchi A, Kakizawa S, Nishi M, Takeshima H. Mice lacking the intracellular cation channel TRIC-B have compromised collagen production and impaired bone mineralization. Sci Signal 2016; 9:ra49
27. Widhe TL. A probable new type of osteopenic bone disease. Pediatr Radiol 2002; 32:447-451
28. Zhou X, Lin P, Yamazaki D, Park KH, Komazaki S, Chen SR, Takeshima H, Ma J. Trimeric intracellular cation channels and sarcoplasmic/endoplasmic reticulum calcium homeostasis. Circ Res 2014; 114:706-716
29. Weber M, Roschger P, Fratzl-Zelman N, Schoberl T, Rauch F, Glorieux FH, Fratzl P, Klaushofer K. Pamidronate does not adversely affect bone intrinsic material properties in children with osteogenesis imperfecta. Bone 2006; 39:616-622
30. Ruffoni D, Fratzl P, Roschger P, Klaushofer K, Weinkamer R. The bone mineralization density distribution as a fingerprint of the mineralization process. Bone 2007; 40:1308-1319
31. Nawrot-Wawrzyniak K, Misof BM, Roschger P, Pańczyk-Tomaszewska M, Ziółkowska H, Klaushofer K, Fratzl-Zelman N. Changes in bone matrix mineralization after growth hormone treatment in children and adolescents with chronic kidney failure treated by dialysis: a paired biopsy study. American Journal of Kidney Diseases 2013; 61:767-777

32. Depalle B, Qin Z, Shefelbine SJ, Buehler MJ. Influence of cross-link structure, density and mechanical properties in the mesoscale deformation mechanisms of collagen fibrils. J Mech Behav Biomed Mater 2015; 52:1-13
33. Xu W, Liu B, Liu X, Chiang MY, Li B, Xu Z, Liao X. Regulation of BMP2-induced intracellular calcium increases in osteoblasts. J Orthop Res 2016; 34:1725-1733
34. Millan JL. The role of phosphatases in the initiation of skeletal mineralization. Calcif Tissue Int 2013; 93:299-306
35. Fujisawa R, Tamura M. Acidic bone matrix proteins and their roles in calcification. Front Biosci (Landmark Ed) 2012; 17:1891-1903
36. de Bruyn JR, Goiko M, Mozaffari M, Bator D, Dauphinee RL, Liao Y, Flemming RL, Bramble MS, Hunter GK, Goldberg HA. Dynamic light scattering study of inhibition of nucleation and growth of hydroxyapatite crystals by osteopontin. Plos One 2013; 8:e56764
37. Bouleftour W, Juignet L, Bouet G, Granito RN, Vanden-Bossche A, Laroche N, Aubin JE, Lafage-Proust MH, Vico L, Malaval L. The role of the SIBLING, Bone Sialoprotein in skeletal biology - Contribution of mouse experimental genetics. Matrix Biol 2016; 52-54:60-77
38. Granito RN, Bouleftour W, Sabido O, Lescale C, Thomas M, Aubin JE, Goodhardt M, Vico L, Malaval L. Absence of bone sialoprotein (BSP) alters profoundly hematopoiesis and upregulates osteopontin. J Cell Physiol 2015; 230:1342-1351
39. Palomo T, Al-Jallad H, Moffatt P, Glorieux FH, Lentle B, Roschger P, Klaushofer K, Rauch F. Skeletal characteristics associated with homozygous and heterozygous WNT1 mutations. Bone 2014; 67:63-70

Figure Legends:

Figure 1: Bone tissue characteristics

Trans-iliac bone biopsy section of P2 under light microscopy (A) shows plump osteoblasts forming an unmineralized matrix (dark gray). Mineralized matrix appears light gray (Goldner's trichrome staining represents originally mineralized bone matrix in green, and osteoid in purple). Active bone formation was very rarely sighted. Backscattered images show bone biopsy samples from P2 (B), P4 (C) and P7 (D). The very low amount of trabecular bone tissue in P7's sample is consistent with his severe skeletal phenotype. Under confocal laser-scanning microscopy, fluorescent double labels are detected on intra- and endocortical bone surfaces (E, see white arrows), which does not reflect high bone remodeling but cortical bone apposition. F) BMDD curves of cancellous bone of the 3 patients in relation to pediatric reference values (20) and to patients with OI type I (23). Note that P4 has very low bone turnover and consequently the BMDD curve was right-shifted, reflecting higher average tissue age of the bone packets.

Figure 2: Proband (P7) osteoblast time curve versus controls, and murine osteoclast differentiation

Osteoblast differentiation time course (from P7) depicting relative levels of RNA transcripts for various proteins involved in collagen synthesis or bone mineralisation, measured at baseline and every 5d, for 30d. RNA transcripts included *RUNX2*, *SP7*, *COL1A1*, *ALPL* (TNSALP), *BGLAP* (osteocalcin), *SPARC* (osteonectin), *OPN* (osteopontin), *IBSP*, *DMP1*, *SOST* and *RANKL*/*OPG*. Murine osteoclast differentiation cultures (bottom panels) were used to measure calcium channel expressions. *Itpr3*/*Ryr3* transcripts are equivalent to those for the human ER calcium efflux channels IP_3R and RyR, and *Tric-b*/*Tric-a* transcripts are equivalent to those for the human channels TRIC-B and TRIC-A.

Table 1 Clinical phenotype of affected patients

Patient	**P1**	**P2**	**P3**	**P4**	**P5**	**P6**	**P7**	**P8**
Sex	Male	Male	Female	Female	Male	Female	Male	Male
Antenatal Scan	Bowed left femur	Normal	Normal	Normal	Normal	Bowed femora	Normal	Normal
Birth weight (kg) at term	2.5	2.7	2.4	2.9	1.8	2.3	3.4	2.64 (34 wks)
Sclera	Grey	White	White	Blue	White	Blue	Blue	White
Age 1st fracture (years)	0.2	2	2	0.3	0.5	0	0	No fractures
Location 1st recorded fracture	Vertebra	Femur	Femur	Femur	Tibia	Femur	Femur	No fractures
Rodding surgery location (age-years; number of operations)	Femur (2.5;1)	Femur (6.9;1)	None	Femur (2.5; 1)	Femur (7;1) Spine (12; 2)	None	Both Femora & right tibia (2-7; 7)	None
Developmental delay	Global	Global	None	None	Motor	Motor	None	None
Hearing loss	Sensorineural	Normal	Normal	Normal	Normal	Normal	Sensorineural	Normal
Scoliosis (Cobb angle˚)	None	None	None	Minimal (4˚)	Moderate (50˚)	None	Moderate (29˚)	Minimal (2˚)
Height Z-score (age, years)	-1.07 (4)	0.2 (14.11)	-1.9 (22)	-2 (22)	-1.27 (14.6)	-1.2 (11.9)	-3 (27)	0.1 (24)
Weight Z-score (age, years)	1.48 (4)	2.6 (14.11)	1.5 (22)	1 (22)	0.01 (14.6)	-0.2 (11.9)	0 (27)	1.5 (24)
BMI Z-score	3.07	2.4	1.9	1.7	0.76	0.6 (11.9)	1	1.5

Table 2 Bone density, fractures and response to bisphosphonate therapy

Patient	**P1**	**P2**	**P3**	**P4**	**P5**	**P6**	**P7**	**P8**
Current age (years)	4	15	26	24	14.9	12	27	24
Lumbar spine BMD Z-score (age in years)	Too young	-3.1 (12)	-0.5 (23)	0.1 (21)	-2.0 (4)	-1.6 (5)	-4.77 (12) *	-1.8 (24)
Lumbar spine BMD Z-score post-BP treatment (duration in years)	N/A	-0.1 (2)	N/A	N/A	-0.3 (6)	N/A	-3.6 (1)	N/A
BP therapy	Pamidronate, Zoledronate	Zoledronate	None	None	Pamidronate, Zoledronate	None	Pamidronate	None
Age started (years)	2	12	N/A	N/A	5	N/A	13	N/A
Number of vertebral fractures (age, years)**	8 (0.2)	13 (11)	None (24)	None (21)	3 (4)	None (12)	None (27)	None (24)
Number of non-vertebral fractures prior to BP treatment (location)	None	4 (femur)	2 (femur, radius)	5 (femur)	5 (tibia, femur, humerus)	2 (femur, tibia)	17 (lower extremity long bones)	None
Number of non-vertebral fractures after BPs started (location)	2 (femur, tibia)	0	N/A	N/A	1 (tibia)	N/A	1 (tibia)	N/A

* lumbar spine QCT density Z-score -2.9; ** age refers to earliest detection in patients with fractures, and latest assessment for those with none

Table 3 Results of bone histomorphometry

Parameters	Control values (15)	Patient 2	Patient 4	Patient 7	OI type I (19)
Age at biopsy (years)	11-13.9	12	12	13	7.6 ± 3.8
Structural parameters					
BV/TV [%]	24.4 ± 4.3	##	17.98	4.46	11.0 ± 5.2
Tb.Th [µm]	148 ± 23	93.43	141.64	53.94	105.0 ± 25
Tb.N. [/mm]	1.66 ± 0.22	##	1.27	0.83	1.3 ± 0.39
Ct. Wi [mm]	0.90 ± 0.33 #	0.81##	0.60	0.56	0.52 ± 0.20
Static parameters of bone formation					
OV/BV [%]	2.12 ± 1.0	4.18	1.97	4.73	5.2 ± 2.6
O.Th [µm]	6.7 ± 1.7	4.55	7.94	3.43	5.5 ± 1.7
OS/BS [%]	22.1 ± 7.8	54.22	17.23	38.08	48 ± 14
ObS/BS [%]	6.7 ± 4.5	2.97	0.96	8.98	19.4 ± 9.5
Dynamic parameters of bone formation					
MS/BS [%]	11.07 ± 5.0	7.05	n.a	9.93	48 ± 16
MAR [µm/d]	0.87 ±0.09	0.92	n.a	0.77	0.73 ± 0.18
Aj. AR [µm/d]	0.46 ± 0.10	0.12	n.a	0.20	0.35 ± 0.14
BFR/BS [µm/y]	37.3 ± 16.7	23.77	n.a	27.75	77 ± 34
BFR/BV [%/y]	49.9 ± 21.4	50.28	n.a	108.18	116 ± 62
Mlt [d]	14.5 ± 3.00	37.88	n.a	17.18	16.5 [12.5 -19.8]
Static parameters of bone resorption					
ES/BS [%]	14.9 ± 5.6	2.94	1.55	0	15.6 [13.7 - 21.8]
Oc.S/BS [%]	1.14 ± 0.74	0.15	0.10	0	1.37 [1.05 - 1.70]
N. Oc/BS [/mm]	0.29 ± 0.14	0.04	0.03	0	0.47 ± 0.29

For comparison, typical values for patients with OI type I are given (19). # Mean value from two cortical plates; ## sample contained only one cortical plate. Therefore, BV/TV and Tb.N could not be assessed. Patient 4 did not receive tetracycline labeling.

Table 4 qBEI results from cancellous and cortical bone

BMDD parameters:	Reference values Controls (20)	P2	P4*	P7 #	P7 post BP treatment	Reference values OI type I (23)
Cancellous bone						
CaMean [wt% Ca]	20.95 (0.57)	20.67	22.09	21.10	-	22.43 (0.63)
CaPeak [wt% Ca]	21.66 (0.52)	21.66	22.87	22.36	-	23.39 (0.57)
CaWidth [Δwt% Ca]	3.47 [3.12; 3.64]	3.64	3.12	2.95	-	3.08 (0.28)
CaLow [%]	6.14 [4.90; 7.99]	9.65	4.43	9.59	-	5.94 (2.05)
CaHigh [%]	0.89 [0.43; 1.47]	1.24	3.54	2.03	-	7.54 [5.00;11.82]
Cortical Bone						
CaMean [wt% Ca]	20.45 [19.68; 21.04]	20.99	21.07	19.04	21.00	22.51 (0.46)
CaPeak [wt% Ca]	21.14 [20.62; 21.75]	21.66	21.92	19.50	21.49	23.29 (0.48)
CaWidth [Δwt% Ca]	3.81 [3.38; 4.38]	3.29	4.42	5.03	3.81	3.28 (0.25)
CaLow [%]	9.06 [6.22; 15.00]	6.53	8.61	27.40	5.32	4.60 (0.80)
CaHigh [%]	0.46 [0.28; 1.22]	0.81	2.33	0.36	0.44	8.60 (4.00)

BMDD reference values for healthy controls (1.5 to 23 years) and OI patients (2 to 14 years) are provided as median [interquartile range] or mean (SD), as appropriate (20,23). Note that the BMDD in healthy children has only minor variation and does not show any age-dependency (20)
*Only one cortex available
High cortical bone formation

Figure1

Click here to download Figure TMEMB38_Fig1v.tif

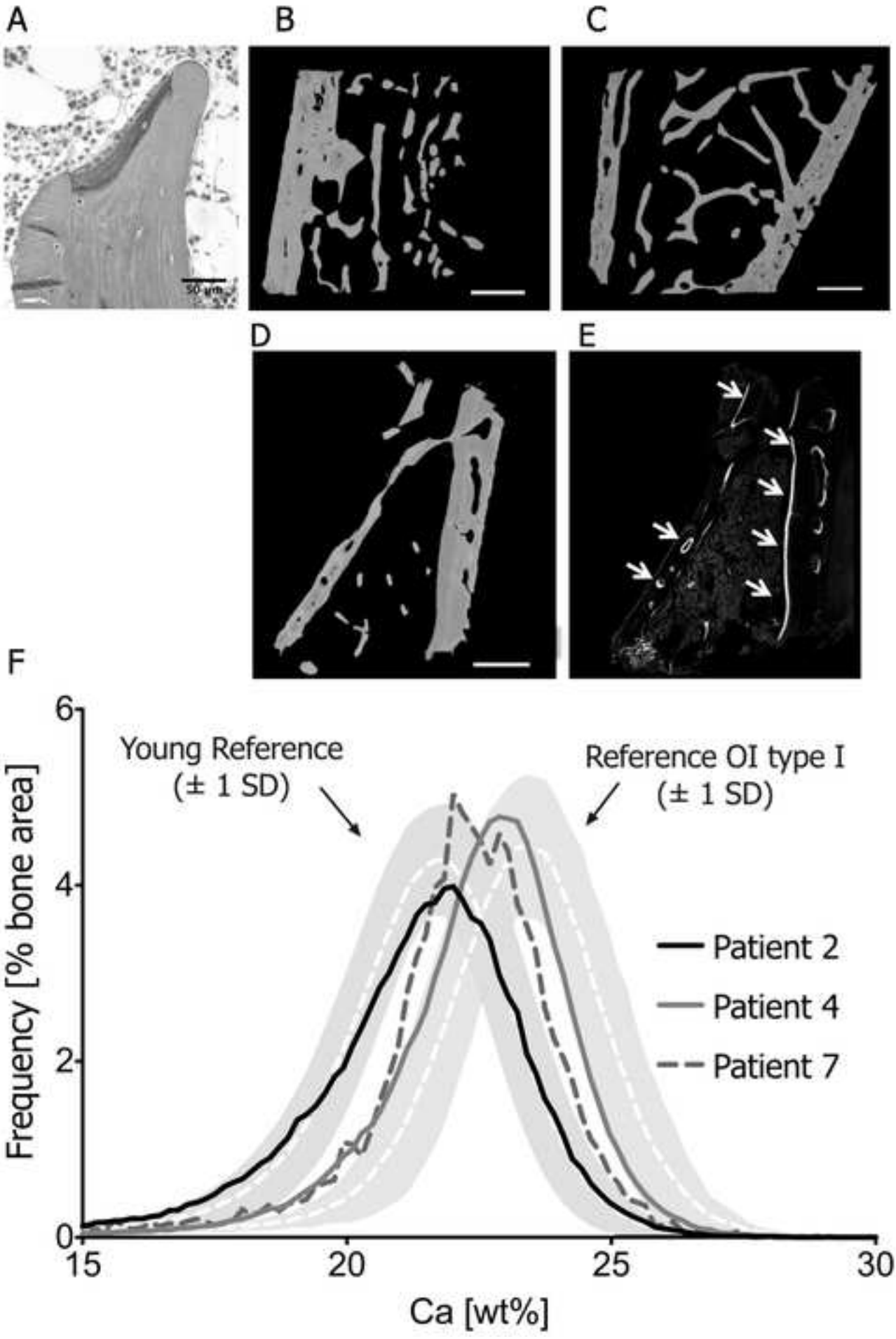

Figure2

Click here to download Figure Figure2.tif

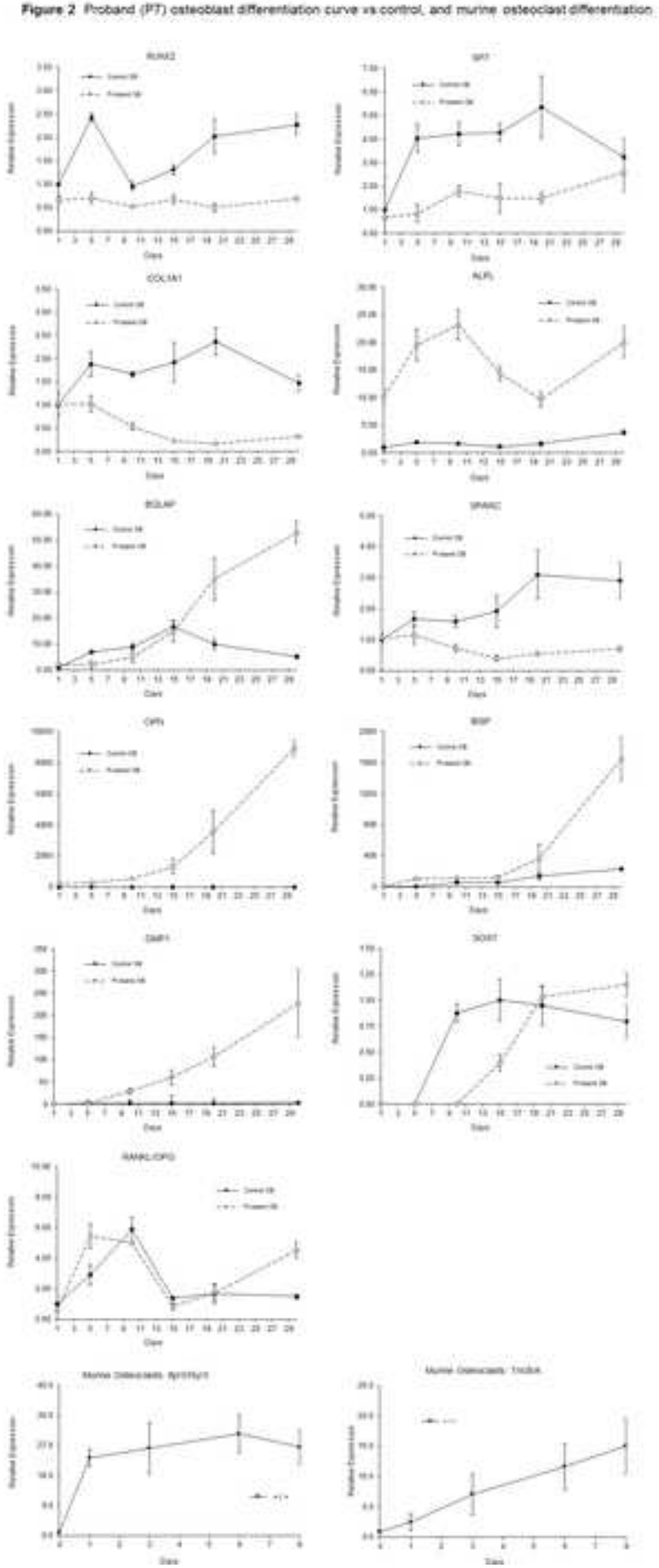

Figure 2 Proband (P7) osteoblast differentiation curve vs control, and murine osteoclast differentiation

Supplemental Figure 1

Supplemental Figure 2